π-π Stacking Mediated Chirality in Functional Supramolecular Filaments

Myungshim Kang[†], **Pengcheng Zhang**[⊥], **Honggang Cui**[§,⊥], and **Sharon M. Loverde**[*,†,‡]

[†]Department of Chemistry, College of Staten Island, The City University of New York, 2800 Victory Boulevard, Staten Island, New York 10314, United States

[‡]Ph.D. Program in Chemistry, Biochemistry, and Physics, The Graduate Center of the City University of New York, New York, New York 10016, United States

[⊥]Department of Chemical and Biomolecular Engineering and Institute for NanoBioTechnology, The Johns Hopkins University, 3400 North Charles Street, Baltimore, Maryland 21218, United States

[§]Department of Oncology and Sidney Kimmel Comprehensive Cancer Center, Johns Hopkins University School of Medicine, Baltimore, Maryland 21205, United States

Abstract

While a great diversity of peptide-based supra-molecular filaments have been reported, the impact of an auxiliary segment on the chiral assembly of peptides remains poorly understood. Herein we report on the formation of chiral filaments by the self-assembly of a peptide-drug conjugate containing an aromatic drug camptothecin (CPT) in a computational study. We find that the chirality of the filament is mediated by the $\pi-\pi$ stacking between CPTs, not only by the well-expected intermolecular hydrogen bonding between peptide segments. Our simulations show that $\pi-\pi$ stacking of CPTs governs the early stages of the self-assembly process, while a hydrogen bonding network starts at a relatively later stage to contribute to the eventual morphology of the filament. Our results also show the possible presence of water within the core of the CPT filament. These results provide very useful guiding principles for the rational design of supramolecular assemblies of peptide conjugates with aromatic segments.
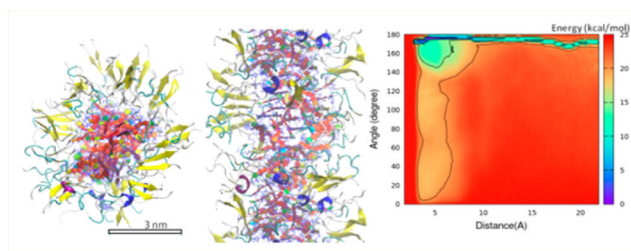
Graphical Abstract

[*]**Corresponding Author**: (S.M.L.), sharon.loverde@csi.cuny.edu. Telephone: 718-982-4075. Fax: 718-982-3910.

Notes
The authors declare no competing financial interest.

INTRODUCTION

Chirality in both functional and biological supramolecular polymers is manifested at multiple length scales.[1−4] For example, chirality in amyloid fibrils can originate at the protofilament or fibril level, but the pitch of amyloid filaments is on the length scale of 100 nm. In comparison, the helicity of the microtubule structure has a pitch of 12 nm. On the synthetic side, rationally designed peptide amphiphiles, can self-assemble into a variety of morphologies: nanofibers, twisted ribbons, nanotubes.[5−11] The pitch of self-assembled supra-molecular assemblies composed by peptide amphiphiles (PAs) can range from several nanometers to hundreds of nanometers. Harnessing control of the pitch and/or shape of these supramolecular polymers for functional biological applications remains a challenge.[12]

Recently, drug amphiphiles (DAs) have been shown to self-assemble into discrete, stable supramolecular filaments with a high and fixed drug loading.[7] Furthermore, the supramolecular nature is more complex than a simple unidimensional assembly; these peptide-drug amphiphiles have been shown to form filaments, nanobelts, nanotubes, and twisted ribbons, exhibiting an inherent chirality and highly ordered structures after initial filament formation.[5−9] DAs like PAs[13,14] are chemically versatile supramolecular systems with great potential as functional nanodelivery vehicles. In particular, DAs incorporate a high loading capacity into their conjugated design and a controlled, yet dynamic supramolecular shape that can be fine-tuned. This strategy harnesses the intrinsic drug−drug interactions (hydrophobicity and $\pi-\pi$ stacking) for the supramolecular design of the drug carrier. Multiple questions have arisen regarding these new assemblies, beginning with the structure and stability of the filaments. Herein, we report the first simulation studies of DAs to probe the delicate balance of underlying forces driving filament self-assembly.

The DA used in this study consists of a β-sheet forming peptide (CGVQIVYKK, or Tau) conjugated to a hydrophobic anticancer drug camptothecin (CPT) via a biodegradable disulfide linker (disulfylbutyrate, buSS), as shown in Figure 1a, mCPT-buSS-Tau. The estimated value of the classic packing parameter[15−19] ($v/a_0 l_c$) for the DA in discussion is 0.29, less than 1/3, predicting a spherical assembly. [Classically, the packing parameter has been suggested to predict and dictate the shapes of self-assembled aggregates (micelles) of amphiphilic molecules such as surfactants or polymers based on their geometric features, including the volume of their hydrocarbon chains, v, the optimal headgroup area, a_0, and the critical chain length l_c. A cylindrical shape is preferred by the amphiphiles with packing parameter of $(1/3) < v/a_0 l_c < (1/2)$, while the amphiphiles with smaller packing parameters would form spherically shaped aggregates.] We obtain this estimate when the rigid CPT and

the linker are used to calculate the critical chain length, l_c, and the volume, v, and the outer surface area is used for the headgroup area, a_0. However, these DAs are observed to form one-dimensional nanostructures. To account for this discrepancy, we need to consider two additional parameters. First, hydrogen bonding is not included in the packing parameter. It has been suggested that the formation of a directional hydrogen bonding network leads to filaments favored over spherical micelles.[20] Second, the planar pentacyclic CPT can $\pi-\pi$ stack, adding to the preference of forming a cylindrical shape over the sphere or bilayer. When CPT planes are perpendicular to the filament, this can facilitate the unidirectional growth of the assembly. The binding energy of $\pi-\pi$ stacking is small but comparable to that of hydrogen bond.[21,22] It has been suggested that $\pi-\pi$ stacking interactions are important in the stabilization of self-assemblies of DNA-templated oligomers, or cooperative assembly of electron donor−acceptor superstructures, along with hydrogen bonding.[23−25] These forces are difficult to account for in simple packing models of self-assembly. Thus, the self-assembly behavior of β-sheet containing amphiphiles cannot be explained using packing parameters based on optimal interfacial area. Likely in some cases, the observed filamentous nanostructures may bear more resemblance to the structural features of amyloid fibrils[26] than that of cylindrical micelles of traditional surfactants, depending on the specific molecular design. It is suggested that β-sheet secondary structure of PAs, which forms hydrogen bonding between peptides perpendicular to the axis of the growth, drives assembly into filaments, as opposed to bilayers or spheres.[27,28] Furthermore, a delicate balance between the hydrophobic interaction, hydrogen bonding, and electrostatics plays a critical role in the lateral growth of the β-sheets and eventually determining the morphology of the self-assembled supramolecular structures.[23,24,28−32]

In order to probe the delicate balance of underlying forces driving filamentous self-assembly, including $\pi-\pi$ stacking and hydrogen bonding, we perform two sets of long-time (~200 ns) large-scale atomistic molecular dynamics (MD) simulations of a DA, mCPT-buSS-Tau. We find that the $\pi-\pi$ stacking between CPTs serves as an anchor for the development of micellar nuclei. Our simulations indicate the potential rearrangement of hydrogen bonding network in the later stage of assembly process to enforce intermolecular interactions and define the eventual morphology. The equilibrated structure of the preassembled filament displays a preferred radial angle of the CPTs supporting a helical packing of CPTs, as is observed in the CD spectrum. Surprisingly, we find water present in the core possibly due to the rigidity of the CPT segments as well as the helical packing of CPTs. Our free energy calculation of two CPTs in solution using multiple walkers metadynamics shows frustration of T-shaped $\pi-\pi$ stacking due to the bent shape of CPT and the additional excluded volume of the peptide. We hypothesize that controlling excluded volume of peptide (and drug) can control the $\pi-\pi$ stacking angle and thus the resulting morphology of the supramolecular assembly. We believe these results provide new insights for understanding and designing functional supramolecular assemblies of peptide conjugates containing aromatic segments.

METHODS

Simulation Systems.

The random system consists of randomly inserted 96 mCPT-buSS-Tau molecules. To build a starting structure of the preassembled system, 6 mCPT-buSS-Tau molecules are placed in each layer with CPTs pointing radially inward for an initial diameter of the fiber of 13.2 nm. The angle between adjacent mCPT-buSS-Tau molecules is 60°. The second layer is identical to the first layer but rotated by 30° relative to the first layer with the distance between the layers of 5 Å. The alternate first and second layers are placed along the fibril axis to form 9 layers in total, resulting in 54 ($6 \times 9 = 54$) mCPT-buSS-Tau molecules, as shown in Figure S1. Both the random system and the preassembled system are solvated in a water box. Each system is neutralized with Cl^-. The total number of atoms for the random and the preassembled system are 969,087 and 111,872, respectively. The concentrations of mCPT-buSS-Tau are 16.2 mM and 122.9 mM in the random and the preassembled system, respectively.

Simulation Procedure.

The force field for the mCPT-buSS-Tau is parametrized using the general AMBER force field (GAFF)[33] with the atomic partial charges on the CPT and the linker assigned by VCharge v1.01[34] (VeraChem, LLC). The TIP3P model[35] is used for water. Atomistic MD simulations of mCPT-buSS-Tau are carried out using NAMD2.[36] All systems use the NPT ensemble and Langevin dynamics[37] at a pressure of 1 atm using Langevin piston method[37,38] with a piston period of 200 fs and a damping time scale of 50 fs at a temperature of 310 K with a damping coefficient $\gamma = 1$ ps^{-1}. Full electrostatic interactions are taken into account, using the particle mesh Ewald (PME) algorithm,[39] with full periodic boundary conditions. The cutoff for van der Waals interactions is 12 Å with a smooth switching function at 10 Å used to truncate the van der Waals potential energy at the cutoff distance. Covalent bonds involving hydrogen are held rigid using the SHAKE algorithm, which allows a 2 fs time step. Coordinates are saved every 2 ps for the postanalysis of the trajectory. Simulations are performed for 220 and 210 ns, for the random and the preassembled system, respectively.

Free Energy Calculation.

The free energy of 2 CPTs as a function of the angle and distance is calculated using multiple walkers metadynamics method.[40] Metadynamics has been successively applied in many fields to sample rare events and to reconstruct the free energy surface. In metadynamics, the dynamics in the space of the chosen collective variables (CVs) is biased by a history-dependent potential. The history-dependent potential is constructed as a sum of Gaussian "hills" centered along the previously explored trajectory. The multiple walkers metadynamics speeds up calculations by employing multiple interacting simulations, called *walkers*. Here we use 10 walkers for 30 ns each. The free energy G is calculated as a function of the following CVs: (i) distance between the centers of C17 and N20 in the CPT planes; (ii) dihedral angle between the CPT planes. The initial height of the Gaussian hills is set to 0.01 kJ/mol. The widths are chosen to be 0.1 Å and 2.5° for the distance and the

dihedral angle, respectively. The deposition time of the biasing Gaussians was fixed to 2 ps. All calculations use NAMD2.[36]

RESULTS AND DISCUSSION

The $\pi-\pi$ stacking between planar CPT moieties is characteristic in self-assembly of mCPT-buSS-Tau. The $\pi-\pi$ stacking between CPTs results from its planar pentacyclic structure. Parts b and c of Figure 1 show the parallel alignments of CPTs during the aggregation in simulation of the random system after 220 ns. In addition to general hydrophobic collapse, this $\pi-\pi$ stacking facilitates initial formation of molecular aggregates, as well as contributes to the stability of the nanostructure, as shown in the preassembled system (Figure 1, parts d and e). The width of the preassembled system after 210 ns simulation is 7.80 ± 0.01 nm (averaged over the last 2 ns of simulation), which has reasonably good agreement with the experimental width of 6.7 ± 1 nm of mCPT-buSS-Tau filaments measured in the transmission electron microscope (TEM) image, as shown in Figure 1f. In comparison, the initial setup of the preassembled filament has a diameter of 13.2 nm. The structure of the filament relaxes significantly after 210 ns. In the circular dichroism (CD) spectrum of mCPT-buSS-Tau (Figure 1g), the negative peaks at 250 nm and 330−400 nm indicate the chiral packing between the CPT moieties, while the negative peak at 216 nm indicate the presence of hydrogen bonds between the β-sheet forming Tau peptides.[7] Hydrogen bonds also play a role in the formation of molecular aggregates, as well as stabilize the final supramolecular nanostructure.

mCPT-buSS-Tau aggregates quickly during first 20 ns, which then proceeds at a gradually slower growth rate over the course of 220 ns in the random system. The number of hydrogen bonds between DAs increases and interaction energies between DAs decreases, as shown in Figure 2. $\pi-\pi$ interactions between CPT moieties act like anchors in early stages of the intermolecular clustering. When the contact distance between any atoms in mCPT-buSS-Tau molecules is less than 4.5 Å, it is considered as a cluster. We regard these clusters as "molecular clusters". To analyze the effect of CPT−CPT interactions on the growth patterns, we define a CPT cluster based on a contact distance of 4.5 Å only between atoms in CPT moieties. The average size of molecular clusters increases, accompanied by a gradual decrease of the number of molecular clusters: the number of molecular cluster decreases from 24 at 20 ns to 15 at 220 ns while the average size of molecular clusters increases from 4 to 6.3 during the same period. In contrast, the number of CPT clusters reaches a plateau more quickly than molecular clusters and they stay stable once formed: about 80% of 15 cluster, the total number of CPT clusters at the end of 220 ns simulation, form within the first 3.2 ns of the simulation. The number of CPT clusters reaches the final value of 15 at 12 ns with a slight fluctuation afterward. Following, the average size of the CPT clusters continues to rapidly increase up to 46 ns. The gradual increase of the average size of CPT clusters after the number of CPT clusters hits a maximum results from aggregate growth (the joining free single DAs to existing CPT clusters), rather than the merging of two or more pre-existing CPT clusters. The ratio between the number of CPT clusters and that of molecular clusters increases from 0.5 at 12 ns to 1.0 at 220 ns due to the decrease of the number of molecular clusters. While the number of molecular clusters decreases, the number of CPT clusters stabilizes early in the simulation. This indicates that the CPTs may not be in

contact when some molecular clusters are merged, resulting in multiple CPT clusters contained in a single molecular cluster.

Moreover, CPTs are not in contact during cluster−cluster merging into a larger aggregate. The hydrophobic CPTs are buried under a shell of charged Tau peptides in the aggregates in the water environment. This suggests an anchor-like role of CPT−CPT interactions in the early stage of aggregation. In addition, the average ratio between the shortest and the longest principle axes decreases as the size of the clusters increases in both the molecular and the CPT clusters, indicating the axial elongation of the clusters, as shown in Figure 2b. The bigger the size of clusters grows, the more elongated their shapes become. The axial elongation of molecular clusters correlates with that of CPT clusters. This means that CPT−CPT interactions, as well as the formation of a hydrogen bonding network, add to the axial stability of the clusters, facilitating the directional growth of the clusters.

In the self-assembled system, the numbers of hydrogen bonds and intermolecular hydrogen bonds per DA in mCPT-buSS-Tau molecules increase for ~100 ns and then reach a plateau at 1.41 hydrogen bonds and 0.65 intermolecular hydrogen bonds per DA, respectively (Figure 2c). Here hydrogen bonds between different mCPT-buSS-Tau molecules are classified as intermolecular hydrogen bonds, while intra-molecular hydrogen bonds are defined hydrogen bonding between atoms within the same mCPT-buSS-Tau molecules. However, both of these numbers are lower than the corresponding numbers for hydrogen bonds and intermolecular hydrogen bonds per DA from the preassembled system, 1.61 hydrogen bonds and 1.24 intermolecular hydrogen bonds per DA, respectively. In particular, the fraction of intermolecular hydrogen bonds increased from 46% in the random system to 77% in the preassembled system, indicating substantial switches from intramolecular hydrogen bonds to intermolecular ones and therefore a potential cooperative rearrangement of the hydrogen bonding network to reach the final nanostructure. The nonbonded interaction between mCPT-buSS-Tau including electrostatic and van der Waals interactions also increases, as shown in Figure 2d. The interaction energy between mCPT-buSS-Tau in the random system is dominated by electrostatic interactions. The electrostatic interactions account for 77% of the total interaction energy between DAs. It is also noticeable that the preassembled system shows a higher contribution of van der Waals interactions (31%) and lower contribution of electrostatic interactions (69%) to the total energy, as compared with the random system. In the preassembled system the total interaction energy per DA is only 2% lower. The relative contribution would change depending on salt concentration.

$\pi-\pi$ stacking of planar CPTs of the adjacent mCPT-buSS-Tau's is distinctive and guides the growth of its self-assembly, along with nonspecific hydrophobic interactions. To analyze the $\pi-\pi$ stacking, we measure distances and dihedral angles between the planar CPT moieties in both the random system and the preassembled nanostructure. Figure 3 displays the distribution of distances and dihedral angles. Given the distances between the π planes at the energy minima, we focus on the CPT−CPT pairs within 7 Å of the final distances compared to their initial orientations, as shown in Figure 3, parts $c−f$. In the random system, the initially randomly distributed angles repopulate and form distinct peaks near 10° and 174°, showing the near parallel packing of CPTs within this distance. In the preassembled nanostructure, the final angles are more broadly populated, but mostly the angles are less

than 30°. We note three important findings for the $\pi-\pi$ stacking of CPTs in mCPT-buSS-Tau molecules. First, the population at or near 90°, corresponding to a T-shaped configuration for the interaction between CPTs, is low in both systems. As the simplest prototype of $\pi-\pi$ stacking, the benzene dimer shows three stacking configurations: displaced parallel, T-shaped and a sandwiched configuration.[21] The potential reasons for the absence of the T-shaped configuration will be discussed later. Second, the small deviation of peaks from 0° is observed in our angle distribution. Configurations with minor variations in angles less than 30° are suggested to be similar in energy by previous theoretical studies.[21] It is also suggested that various substituent effects on the relative stability of stacking.[41,42] Third, the favorable London dispersion interactions and, therefore, $\pi-\pi$ stacking may be underestimated with the fixed partial charges in the classical MD force field.[43,44] London dispersion interactions are originated from instantaneous multipole/induced multipole charge fluctuations, which make it essential to describe the polarizability accurately. The previous studies with molecular mechanics force fields slightly underestimated $\pi-\pi$ interactions.[43–45] It was also suggested that $\pi-\pi$ interactions in water have higher energy minimum than that of the solvent-free state due to the damping by solvent competition and the entropic effects.[35,43,45] This may explain why the stacking arrangements are not well-defined in the filament system.

The T-shaped configuration is not observed between CPTs of mCPT-buSS-Tau's in the random system or nanofilament. In order to determine if this is an effect of the additional excluded volume of the peptide chain, we calculate the energy of 2 CPTs as a function of the dihedral angle and distance using multiple walkers metadynamics.[40] We perform multiple walkers metadynamics calculations with 10 different starting configurations for 30 ns each. Distances are measured between the centers of C17 and N20 in the CPT planes (see also the Methods for detail). Dihedral angles are defined between the CPT planes. The calculated interaction free energy of 2 CPTs as a function of angle and distance (Figure 4) displays only two minima: the sandwiched and the displaced parallel configurations. The former has the second lowest energy well of −22.1 kcal/mol at a distance of 4.15 Å and angle 173.75°, while the latter possesses the lowest interaction energy of −24.2 kcal/mol at 4.55 Å and 176.25°. In addition, the latter extends up to the distance of 12 Å. Notably, we do not observe an energy minimum for a T-shaped configuration between the two CPTs. This may be a result of the relatively increased stacking distance between the pentacyclic rings due to the bent shape and the out-of-plane atoms, including the ethyl and hydroxyl groups. The T-shaped minima is not determined in π stackings with various substituents.[46] Additionally, this kind of stacking configuration is not expected to be seen in mCPT-buSS-Tau because of the bulky peptide groups attached to the drug. We hypothesize that controlling excluded volume of peptide (and drug) can control the $\pi-\pi$ stacking angle, and thus the resulting morphology of the supramolecular assembly.

The radial density for the nanofilament after 210 ns shows that CPTs moieties remain buried in the core of the filament, while the hydrophilic peptide groups wrap around the core, forming the outer shell (Figure 5). The positively charged side chains of two Lysine residues at the end of the peptide group preferentially populate at the outermost layer, forming an interface with water, where the charged group is neutralized by Cl$^-$ ions (Figure S2). The

terminus of positively charged amino acid residues such as Lysine is known to be important in self-assembling of short peptides.[47]

Surprisingly, a small peak of water molecules was observed within the core of the CPT filament (Figure S3), suggesting the possible presence of a hollow channel within the 1D nanostructures. The observation is in sharp contrast with nanostructure formed by self-assembly of peptide amphiphile containing linear hydrocarbons, which have been shown to possess a more tightly packed core and no room for water due to the flexibility of the linear hydrocarbons.[27] We speculate the presence of a hollow channel is likely due to the rigidity of CPT segments as well as the helical packing of CPTs. To test this, we synthesize a PA with a C8 linear hydrocarbon (C8-Tau), and test this by preassembling a nanofiber composed of this PA (see Figure S3). Our simulation results do not show any indication of water in the center of the core−shell fiber of C8-Tau.

To further analyze the nanostructure, we calculate the orientation of the CPTs in the core of the nanofilament. The probability distribution of the angle formed between the CPT's long axis (C24−N14) and the radial direction, from the center of the filament to the center of CPT, displays a peak around 22°. The CPT is not oriented in a perfectly radial manner, but displays a preferred angle of rotation around the center of mass. Given the rigid and long pentacyclic structure of CPTs, this results in a cylindrical packing with a hollow cavity in the core the structure, which is occupied by water. It also supports the chiral packing of CPTs, as indicated in the CD spectrum of mCPT-buSS-Tau (Figure 1f). Although the starting configuration has no chirality, after ~200 ns the CPTs align into strands with a predominantly right-handed helical pitch (Figure S4). A packing of single-handed helix columns irrespective of the chirality of their molecular building blocks has been reported in the self-assembly of a family of perylene bismide derivatives.[48] Further analysis of the CPT strands indicates the average length of ~20 Å. Given a longer simulation time, the helicity of the strands could become fully periodic.

The probability distribution of the angle formed between the peptides' longest axis (CA of CYS-CA of LYS (11)) and the radial vector significantly deviates from 0°. The peptides also display a preferred rotation angle around the center of mass of the nanofilament.

It is consistent with the previous IR studies and the proposed helical model based on them.[20] Given that a radial orientation is typical in amphiphilic molecules, the bulky and rigid CPTs, and the resulting $\pi-\pi$ interactions break the symmetry of the radial pattern and orient the molecules at a preferred angle around the center of mass. The end-to-end distances of peptides between CA's of terminal residues displays a broad distribution, indicating various folding states of the peptide, including β-sheets. It has been reported that the propensity for β-sheet formation affects the internal dynamics of the nanofilaments.[49]

CONCLUSION

We investigate the self-assembly mechanism and nanofilament structure of mCPT-buSS-Tau in water using long-time atomistic MD simulations. The planar CPTs in mCPT-buSS-Tau form $\pi-\pi$ stacking in the early stages of the aggregation and serve as anchors for the

development of cluster nuclei in the random system. The clusters tend to elongate as they grow. The ratio of intermolecular hydrogen bonds to the total hydrogen bonds in the preassembled system suggests a cooperative rearrangement in the hydrogen bonding network surrounding the DAs before forming the nanofilament structure. Compared to the random system, the preassembled system has a greater van der Waals interaction and smaller electrostatic interaction between DAs, while the total interaction energies per DA are similar. The $\pi-\pi$ stacking of CPTs of mCPT-buSS-Tau in proximity is distinct and shows both the displaced parallel and sandwiched configurations. The free energy surface calculated using multiple walkers metadynamics of two CPTs also shows energy minima at these two configurations, without a minimum at a T-shaped configuration, possibly due to the bent configuration of CPT. The radius of the core−shell nanostructure of the preassembled system is consistent with experimental observations, but also surprisingly suggests the presence of water in the core. Moreover, the tilting of the axis of long rigid CPT moieties from the radial vector supports chiral packing of CPTs as is indicated in the CD spectrum.

This is the first molecular simulation study of peptide amphiphiles with conjugated aromatic rings including long time all-atomistic simulations of self-assembly and preassembled supramolecular structures, as well as multiple walker metadynamic calculations of aromatic ring stacking. These all-atomistic simulations provide the basis for chemically accurate coarse-grained models that can capture the transition process from elongated micellar aggregates to complete supramolecular nanofilaments. In addition to elucidating the self-assembly behavior of peptide amphiphiles with aromatic rings, these results also elucidate the role of $\pi-\pi$ stacking in mediating chirality in functional supramolecular filaments.

Supplementary Material

Refer to Web version on PubMed Central for supplementary material.

ACKNOWLEDGMENTS

REFERENCES

(1). Ziserman L; Lee HY; Raghavan SR; Mor A; Danino DJ Am. Chem. Soc 2011, 133, 2511−2517.

(2). Miyauchi M; Takashima Y; Yamaguchi H; Harada AJ Am. Chem. Soc 2005, 127, 2984−2989.

(3). Besenius P; Portale G; Bomans PHH; Janssen HM; Palmans ARA; Meijer EW Proc. Natl. Acad. Sci. U. S. A 2010, 107, 17888−17893. [PubMed: 20921365]

(4). Kurouski D; Lu XF; Popova L; Wan W; Shanmugasundaram M; Stubbs G; Dukor RK; Lednev IK; Nafie LA J. Am. Chem. Soc 2014, 136, 2302−2312. [PubMed: 24484302]

(5). Cheetham AG; Ou Y-C; Zhang P; Cui H Chem. Commun 2014, 50, 6039−6042.

(6). Cheetham AG; Zhang P; Lin YA; Lin R; Cui HJ Mater. Chem. B 2014, 2, 7316−7326.

(7). Cheetham AG; Zhang PC; Lin YA; Lock LL; Cui HG J. Am. Chem. Soc 2013, 135, 2907−2910. [PubMed: 23379791]

(8). Lin R; Cheetham AG; Zhang P; Lin Y.-a.; Cui, H. Chem. Commun 2013, 49, 4968−4970.

(9). Lin Y-A; Cheetham AG; Zhang P; Ou Y-C; Li Y; Liu G; Hermida-Merino D; Hamley IW; Cui H ACS Nano 2014, 8, 12690−12700. [PubMed: 25415538]

(10). Chen YR; Gan HX; Tong YW Macromolecules 2015, 48, 2647−2653.

(11). Fleming S; Ulijn RV Chem. Soc. Rev 2014, 43, 8150−8177. [PubMed: 25199102]

(12). Aida T; Meijer EW; Stupp SI Science 2012, 335, 813−817. [PubMed: 22344437]

(13). Hartgerink JD; Beniash E; Stupp SI Science 2001, 294, 1684−1688. [PubMed: 11721046]

(14). Hartgerink JD; Beniash E; Stupp SI Proc. Natl. Acad. Sci. U. S. A 2002, 99, 5133−5138. [PubMed: 11929981]

(15). Israelachvili JN Intermolecular & Surface Forces; 3rd ed.; Academic Press: San Diego, CA, 2011; pp 535−568.

(16). Israelachvili JN; Mitchell DJ; Ninham BWJ Chem. Soc., Faraday Trans. 2 1976, 72, 1525−1568.

(17). Bourov GK; Bhattacharya AJ Chem. Phys 2003, 119, 9219−9225.

(18). Khalil RA; Zarari A-HA Appl. Surf. Sci 2014, 318, 85−89.

(19). Tanford C The Hydrophobic Effect; Wiley: New York, 1973; p 1980.

(20). Paramonov SE; Jun HW; Hartgerink JD J. Am. Chem. Soc 2006, 128, 7291−7298. [PubMed: 16734483]

(21). Hobza P; Selzle HL; Schlag EW J. Am. Chem. Soc 1994, 116, 3500−3506.

(22). Sinnokrot MO; Valeev EF; Sherrill CD J. Am. Chem. Soc 2002, 124, 10887−10893. [PubMed: 12207544]

(23). Paolantoni D; Rubio-Magnieto J; Cantel S; Martinez J; Dumy P; Surin M; Ulrich S Chem. Commun 2014, 50, 14257− 14260.

(24). Surin M; Janssen PGA; Lazzaroni R; Leclere P; Meijer EW; Schenning A Adv. Mater 2009, 21, 1126−1130.

(25). Ley D; Guzman CX; Adolfsson KH; Scott AM; Braunschweig AB J. Am. Chem. Soc 2014, 136, 7809−7812. [PubMed: 24846757]

(26). Morriss-Andrews A; Shea J-E Annu. Rev. Phys. Chem 2015, 66, 643−666. [PubMed: 25648485]

(27). Lee OS; Stupp SI; Schatz GC J. Am. Chem. Soc 2011, 133, 3677−3683. [PubMed: 21341770]

(28). Velichko YS; Stupp SI; de la Cruz MO J. Phys. Chem. B 2008, 112, 2326−2334. [PubMed: 18251531]

(29). Capito RM; Azevedo HS; Velichko YS; Mata A; Stupp SI Science 2008, 319, 1812−1816. [PubMed: 18369143]

(30). Tsonchev S; Schatz GC; Ratner MA J. Phys. Chem. B 2004, 108, 8817−8822.

(31). Tekin ED RSC Adv. 2015, 5, 66582−66590.

(32). Fu IW; Markegard CB; Nguyen HD Langmuir 2015, 31, 315−324. [PubMed: 25488898]

(33). Wang JM; Wolf RM; Caldwell JW; Kollman PA; Case DA J. Comput. Chem 2004, 25, 1157−1174. [PubMed: 15116359]

(34). Gilson MK; Gilson HSR; Potter MJ J. Chem. Inf. Model 2003, 43, 1982−1997.

(35). Jorgensen WL; Chandrasekhar J; Madura JD; Impey RW; Klein ML J. Chem. Phys 1983, 79, 926−935.

(36). Phillips JC; Braun R; Wang W; Gumbart J; Tajkhorshid E; Villa E; Chipot C; Skeel RD; Kale L; Schulten KJ Comput. Chem 2005, 26, 1781−1802.

(37). Martyna GJ; Tobias DJ; Klein ML J. Chem. Phys 1994, 101, 4177−4189.

(38). Feller SE; Zhang Y; Pastor RW; Brooks BR J. Chem. Phys 1995, 103, 4613−4621.

(39). Darden T; York D; Pedersen LJ Chem. Phys 1993, 98, 10089−10092.

(40). Raiteri P; Laio A; Gervasio FL; Micheletti C; Parrinello MJ Phys. Chem. B 2006, 110, 3533−3539.

(41). Hunter CA; Sanders JK M. J. Am. Chem. Soc 1990, 112, 5525−5534.

(42). Masoodi HR; Zakarianezhad M; Bagheri S; Makiabadi B; Shool M Chem. Phys. Lett 2014, 614, 143−147.

(43). Chipot C; Jaffe R; Maigret B; Pearlman DA; Kollman PA J. Am. Chem. Soc 1996, 118, 11217−11224.

(44). Jorgensen WL; Severance DL J. Am. Chem. Soc 1990, 112, 4768−4774.

(45). Gamieldien MR; Strumpfer J; Naidoo KJ J. Phys. Chem. B 2012, 116, 324−331. [PubMed: 22107442]

(46). Mikulski D; Eder K; Molski M Comput. Theor. Chem 2014, 1046, 118−125.

(47). Santana H; Avila CL; Cabrera I; Paez R; Falcon V; Pessoa A, Jr; Ventosa N; Veciana J; Itri R; Souza Barbosa LR Soft Matter 2014, 10, 9260−9269. [PubMed: 25325399]

(48). Roche C; Sun H-J; Leowanawat P; Araoka F; Partridge BE; Peterca M; Wilson DA; Prendergast ME; Heiney PA; Graf R; Spiess HW; Zeng X; Ungar G; Percec V Nat. Chem 2015, 8, 80. [PubMed: 26673268]

(49). Ortony JH; Newcomb CJ; Matson JB; Palmer LC; Doan PE; Hoffman BM; Stupp SI Nat. Mater 2014, 13, 812−816. [PubMed: 24859643]
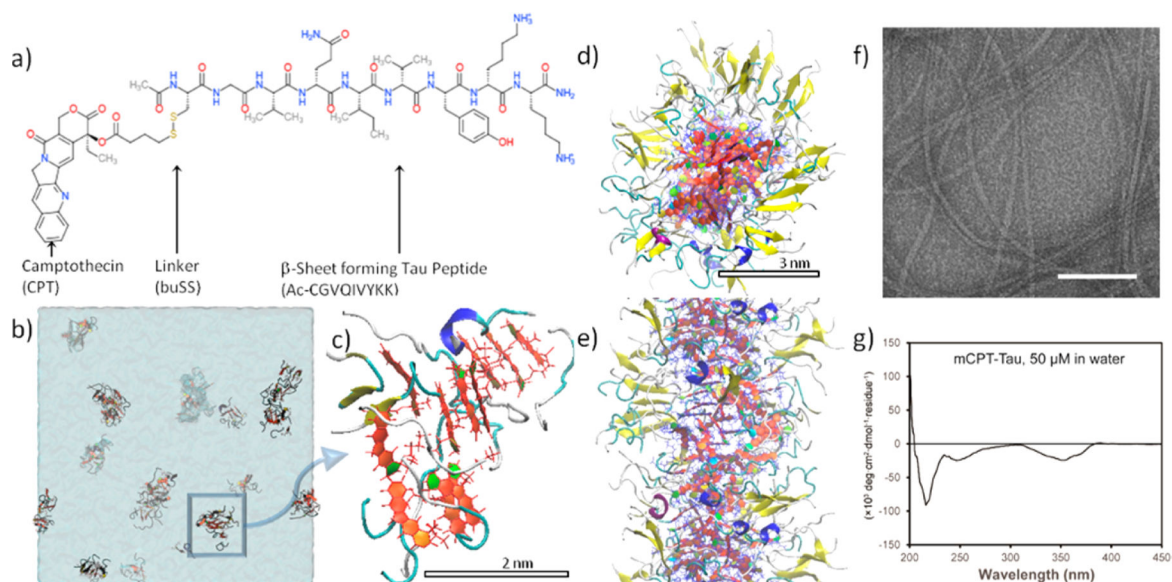
Figure 1.
Self-assembly of mCPT-buSS-Tau. (a) Structure of mCPT-buSS-Tau. (b) Snapshot from molecular dynamics simulation of mCPT-buSS-Tau self-assembly of 16.2 mM random system after 220 ns. (c) $\pi-\pi$ stacking between planar CPTs in a cluster. To show pairs of parallel alignment between CPTs in a cluster clearly, the cluster is rotated. CPT is shown in a licorice and paperchain (orange) representation. The random peptide chains are displayed in white and cyan, indicating coil and turn, respectively. Helices are displayed in blue, while β sheets are shown in yellow. (d and e) Top (d) and side (e) views of a 122.9 mM preassembled filament after 210 ns, respectively. (f) Transmission electron microscope (TEM) image of mCPT-buSS-Tau. Filaments with the width of 6.7 ± 1 nm were observed. The scale bar represents a distance of 100 nm. (g) The circular dichroism (CD) spectrum of mCPT-buSS-Tau. The negative peaks at 250 nm and 330−400 nm indicated the chiral packing between the CPT moieties, while the negative peak at 216 nm indicated the presence of hydrogen bond between the β-sheet forming Tau peptides. The characterization of the assembly using CD and TEM has been described in ref 7.
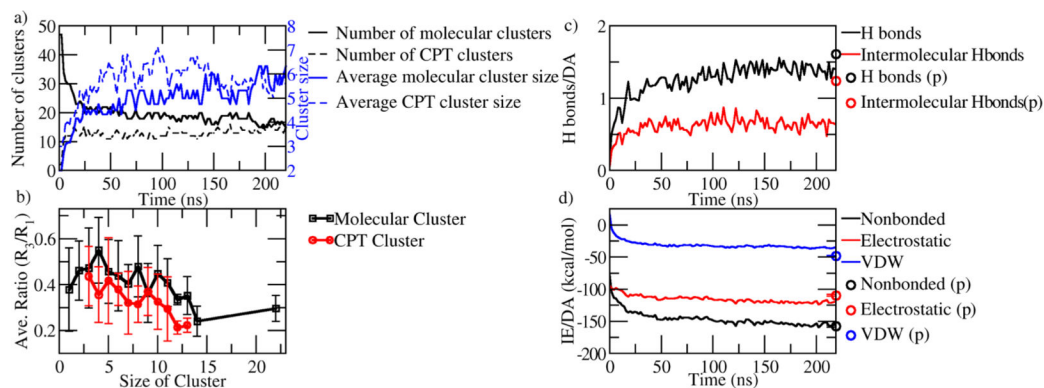
Figure 2.
Aggregation of mCPT-buSS-Tau over time. (a) Number of clusters and the average cluster size over time in nanoseconds. (b) Elongation of clusters. The longest (R1) and shortest principle axes (R3) of clusters were calculated to determine their shape. The average ratio R3/R1 decreased as the size of clusters increased, indicating elongation of clusters. (c) Numbers of hydrogen bonds per DA (H bonds, black solid line) and the intermolecular H bonds per DA (red solid line) increase. The numbers of H bonds per DA (black circle) and intermolecular H bonds per DA (red circle) in the preassembled model (p) are displayed for comparison. (d) Nonbonded interaction energy per DA (black solid line) over time. The energy is decomposed into electrostatic (red solid line) and van der Waals (VDW, blue solid line) contributions. The corresponding interaction energies in the preassembled model (p) are displayed in the empty circle with the matching colors. VDW interaction shows a greater increase over time.
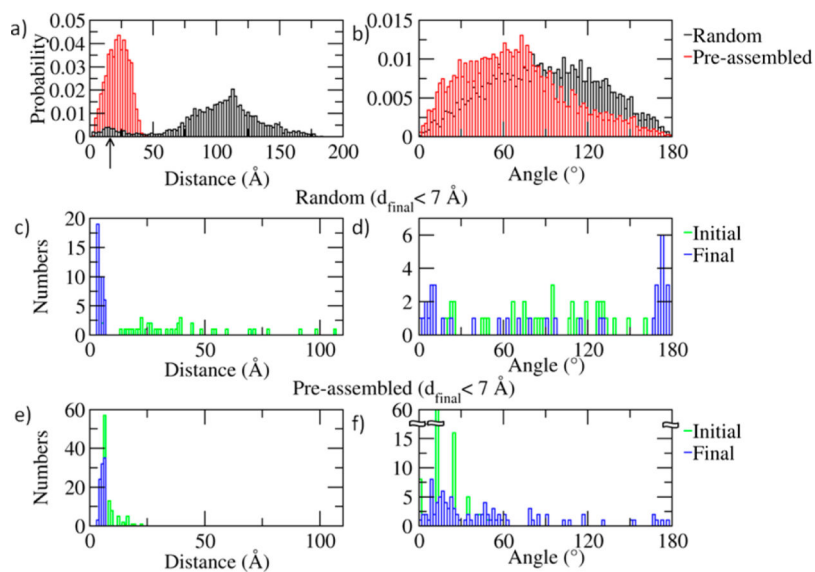
Figure 3.
Stacking of CPTs in mCPT-buSS-Tau random and preassembled system. (a) Distribution of distances between pairs of CPT planes in mCPT-buSS-Tau. (b) Dihedral angle distribution between pairs of CPT planes. (c and d) Initial and final distribution of distance (c) and dihedral angle (d) of selected CPT pairs that have the final distance less than 7 Å in the random system. Peaks near 0° and 180° are distinct, showing the parallel packing within in this distance. (e and f) Initial and final distribution of distance (e) and angle (f) of selected CPT pairs that have the final distance less than 7 Å in the preassembled system. The final angles are more broadly populated, but mostly the angles are less than 30°.
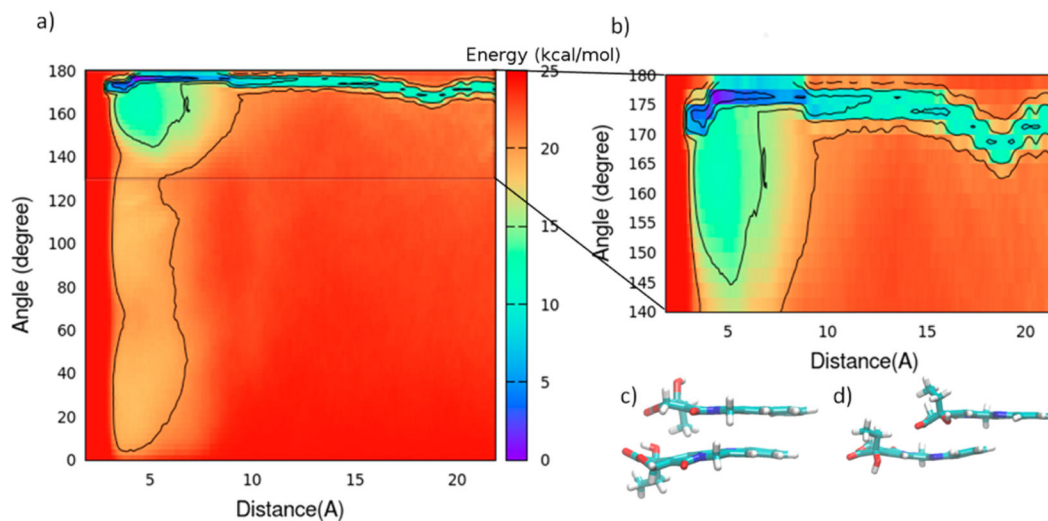
Figure 4.
Free energy of 2 CPTs calculated using multiple walkers metadynamics. (a) Free energy in the function of distance and dihedral angle between 2 CPTs. (b) Two energy minima (expanded). (c) Sandwiched stacking. (d) Displaced parallel stacking. Distances are measured between the centers of C17 and N20 in the CPT planes. Dihedral angles are defined between the CPT planes.
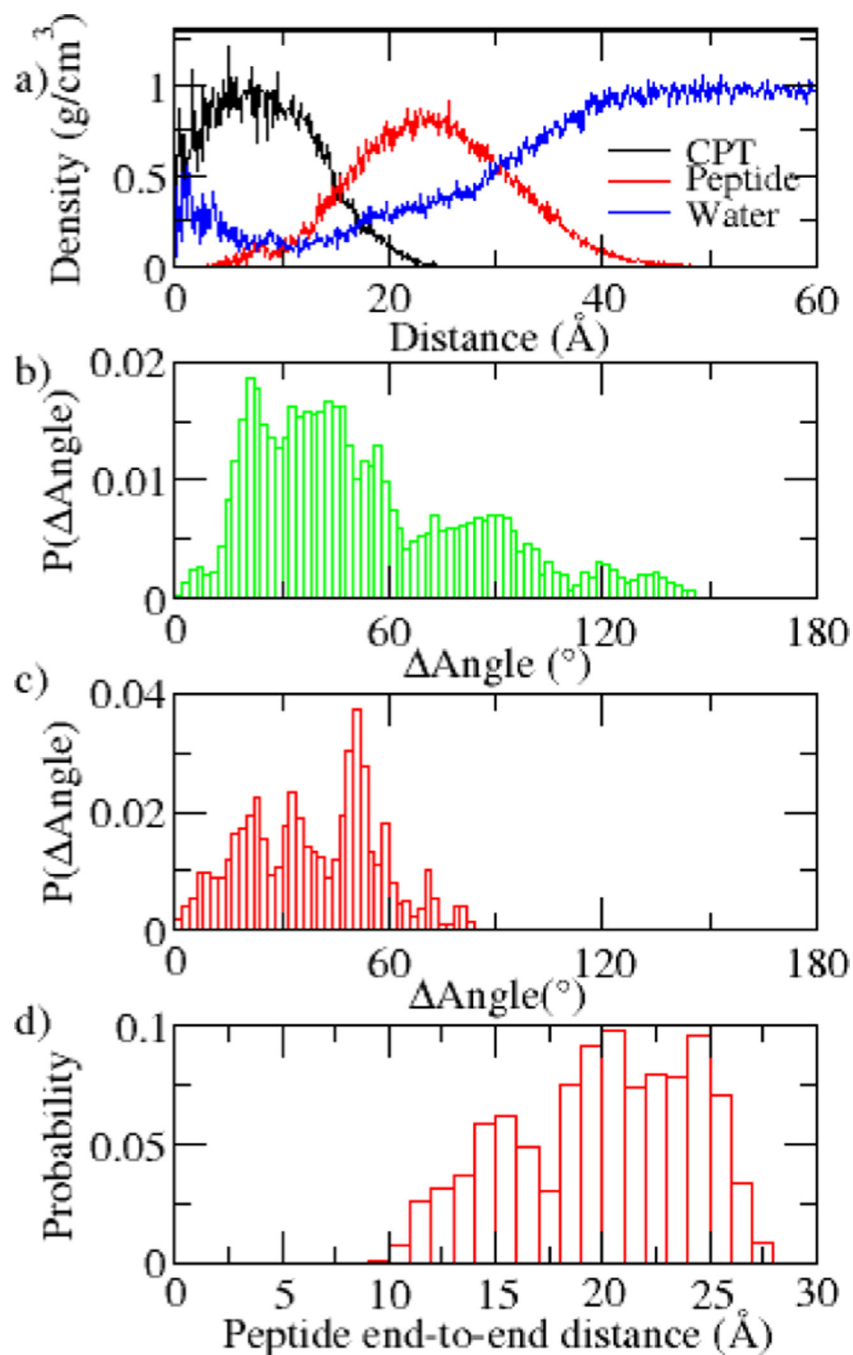
Figure 5.
Structure of preassembled system. (a) Radial distributions in the preassembled system after 210 ns. The density is averaged in the last 2 ns (10 frames). CPTs (black) remain buried in the core of the assembly, while the peptides (red) wrap around the core, forming the outer shell. A small number of water molecules (blue) are observed in the core. (b) Probability density distribution of the angle formed between the CPT's long axis (C24−N14) and the radial direction, from the center of the filament to the center of CPT. (c) Probability density distribution of the angle formed between the peptides' longest axis (CA of CYS-CA of LYS

(11)) and the radial vector. (d) Probability distribution of the end-to-end distances of peptides between CA's of end residues.